Journal Pre-proof

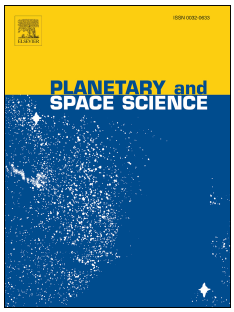

An empirical model of the Earth's bow shock based on an artificial neural network

G. Pallocchia, L. Trenchi

PII: S0032-0633(21)00035-0

DOI: https://doi.org/10.1016/j.pss.2021.105196

Reference: PSS 105196

To appear in: *Planetary and Space Science*

Received Date: 3 August 2020

Revised Date: 9 January 2021

Accepted Date: 25 February 2021

Please cite this article as: Pallocchia, G., Trenchi, L., An empirical model of the Earth's bow shock based on an artificial neural network, *Planetary and Space Science*, https://doi.org/10.1016/j.pss.2021.105196.

Giuseppe Pallocchia: Ideas; formulation or evolution of overarching research goals and aims; Application of statistical, mathematical, computational, or other formal techniques to analyze or synthesize study data; Programming, software development; designing computer programs; implementation of the computer code and supporting algorithms; testing of existing code components;Preparation, creation and/or presentation of the published work, specifically writing the initial draft (including substantive translation)

Lorenzo Trenchi: Application of statistical, mathematical, computational, or other formal techniques to analyze or synthesize study data

Abstract

All of the past empirical models of the Earth's bow shock shape were obtained by best-fitting some given surfaces to large collections of observed crossings. However, the issue of bow shock modelling can be addressed by means of artificial neural networks (ANN) as well. The ANN approach is powerful and flexible since an ANN can capture the hidden relation between the bow shock position and a set of given inputs and forecast its response on the basis of the inputs only.
In this paper we present a perceptron, a simple feedforward network, which computes the bow shock radial position, along a given direction, using as inputs: the two angular coordinates of that direction; the bow shock radial distance R_{F79} provided by Formisano's model (F79) (Formisano, 1979) and the upstream Alfvénic Mach's number Ma .
The perceptron output can be regarded as a correction to the F79 representation of the bow shock shape. A statistical analysis, performed over a test data set of 944 bow shock crossings from several spacecraft, demonstrates that the ANN predictions are effectively more accurate than F79 ones. Indeed, the ANN mean value of the ratio between predicted and observed shock radial distance r_{ANN} is generally closer to the expected value $\mu_r = 1$ than the corresponding r_{F79}. Such improvement on F79 is partly due to the addition of Ma to the model inputs. However, the statistical error σ_{rANN} is practically the same as that from an identical network but with no Ma input line. In this regard, we discuss the possibility that an irreducible uncertainty in predictions originates from the bow shock motions related to the impacts of interplanetary discontinuities on the magnetosphere.

An empirical model of the Earth's bow shock based on an artificial neural network

G. Pallocchia[a,*], L. Trenchi[b]

[a]*Istituto Nazionale di Astrofisica - Istituto di Astrofisica e Planetologia Spaziali, Via del Fosso del Cavaliere 100, Rome (Italy)*
[b]*Serco for ESA, European Space Agency, ESRIN, Directorate of Earth Observation Programmes, Largo G. Galilei 1, Frascati (Italy)*

Abstract

All of the past empirical models of the Earth's bow shock shape were obtained by best-fitting some given surfaces to large collections of observed crossings. However, the issue of bow shock modelling can be addressed by means of artificial neural networks (ANN) as well. The ANN approach is powerful and flexible since an ANN can capture the hidden relation between the bow shock position and a set of given inputs and forecast its response on the basis of the inputs only.

In this paper we present a perceptron, a simple feedforward network, which computes the bow shock radial position, along a given direction, using as inputs: the two angular coordinates of that direction; the bow shock radial distance R_{F79} provided by Formisano's model (F79) (Formisano, 1979) and the upstream Alfvénic Mach's number M_a.

The perceptron output can be regarded as a correction to the F79 representation of the bow shock shape. A statistical analysis, performed over a test data set of 944 bow shock crossings from several spacecraft, demonstrates that the ANN predictions are effectively more accurate than F79 ones. Indeed, the ANN mean value of the ratio between predicted and observed shock radial distance $\overline{r}_{ANN}$ is generally closer to the expected value $\mu_r = 1$ than the corresponding $\overline{r}_{F79}$.

*Corresponding author
Email address: giuseppe.pallocchia@inaf.it (G. Pallocchia)

Such improvement on F79 is partly due to the addition of M_a to the model inputs. However, the statistical error $\sigma_{r_{ANN}}$ is practically the same as that from an identical network but with no M_a input line. In this regard, we discuss the possibility that an irreducible uncertainty in predictions originates from the bow shock motions related to the impacts of interplanetary discontinuities on the magnetosphere.

Keywords: Bow shock
Magnetosphere
Solar wind interactions
Artificial neural networks
`elsarticle.cls`, LaTeX, Elsevier, template
2010 MSC: 00-01, 99-00

1. Introduction

The bow shock, the outer boundary of the Earth's magnetosphere, is a detached shock formed by the interaction of the solar wind flow with the obstacle of the terrestrial magnetic field. When the supersonic solar wind passes through such discontinuity, it is deflected, heated and slowed down to subsonic speed. The bow shock is a dynamic boundary which changes its shape and position according to the different solar wind conditions (e.g., Binsack and Vasyliunas, 1968). The knowledge of the bow shock position can help in practical analysis of processes taking place in the entire magnetic environment of the Earth. During the past half century, several theoretical and empirical models were developed to describe the bow shock shape and its dependence on the upstream solar wind parameters (Fairfield, 1971; Formisano, 1979; Nemecek and Safrankova, 1991; Farris and Russell, 1994; Cairns and Grabbe, 1994; Peredo et al., 1995; Verigin et al., 2001; Jeřáb et al., 2005).

The pioneering two-dimensional model was obtained by best-fitting a hyperbola to bow shock crossings near the ecliptic plane collected by six IMP spacecraft (Fairfield, 1971). Formisano (1979) was the first to provide a three-dimensional

model (hereafter shortened as F79) by best-fitting a second order surface (depending on the solar wind ram pressure P_{ram}) to a large data set of crossings which comprised also the unique very high-latitude observations from HEOS-2 spacecraft. Nemecek and Safrankova (1991) modified the F79 model using a small data set of crossings collected by Prognoz 10 and IMP-8 spacecraft in order to take into account, in addition to P_{ram}, also the magnetosonic Mach's number M_{ms} and the interplanetary magnetic field (IMF) intensity B. Afterwards, Peredo et al. (1995) developed an empirical three-dimensional model using a large number of crossings collected by many spacecraft during over one and a half solar cycles. Those authors found out that the Alfvénic Mach's number M_a influenced the bow shock position more strongly than the sonic M_s or the magnetosonic Mach's number M_{ms}.

On the basis of some bow shock observations and theoretical considerations, Farris and Russell (1994) proposed instead a semi-empirical model derived from a modification of the empirical formulas proposed by Seiff (1962) and Spreiter et al. (1966). In that model the bow shock standoff distance was expressed as a function of both the sonic Mach's number and the radius of curvature of the magnetopause.

Cairns and Grabbe (1994) developed a MHD theory for the bow shock standoff distance and the magnetosheath thickness. Those two parameters were expressed, then, by Cairns and Lyon (1995) as functions of the angle between the solar wind velocity and IMF direction, M_a and M_s.

A comparison of the prediction capability of several bow shock models was performed by Merka et al. (2003) over a large collection of IMP8 bow shock crossings. An important result of that study was that the F79 model provided the best results over the whole data set.

Finally, Merka et al. (2005) improved the Peredo et al. (1995) model while using their original data set and methodology but applying a different error analysis to the fitting method. Those authors found that the revised model was more accurate than all of those discussed in Merka et al. (2003).

We present here an empirical model of the bow shock based on an Artificial

Neural Network (ANN), viz, according to a classical definition, "a computing system made up of a number of simple, highly interconnected processing elements, which process information by their dynamic state response to external inputs"(Caudill, 1989). The processing elements are called "units"and their connections "weights"or, in analogy with the neuroscience terminology, "neurons"and "synapses"respectively. Each unit transforms its weighted inputs into an output by means of a given activation function which can be linear or nonlinear and take different forms. The suitable connection weights to perform a desired computation are found through a process called "learning". The units are organized in layers and generally an ANN consists of one input layer, one output layer and a number of intermediate "hidden"layers. The architecture of an ANN is defined by specifying the connection type (such as recurrent or partially recurrent, feedforward etc.), the learning rule (such as supervised learning, hebbian learning, competitive learning etc.) and the activation functions (such as hyperbolic tangent, sigmoidal, threshold etc.) (e.g., Hertz et al., 1991).

An ANN has two very appealing features which is useful to highlight. The first is that an ANN is a powerful tool to capture (as result of the learning process) the hidden relations of an input-output system and provide its response on the basis of the input only. In addition, an ANN sufficently complex is able to approximate any continuous function (Cybenko, 1989; Hornik et al., 1989).

The aim of this work is to illustrate an alternative approach to the traditional method of best-fitting a given surface to a set of observed crossings and to provide, at the same time, a satisfactory algorithm for the prediction of the shock position. In the following sections, first we briefly describe the particular ANN chosen for this study along with the learning method used to get its connections weights. Afterwards, we discuss the results of the statistical comparison between F79 and our model and summarize the results of the study. Finally, we provide in the Appendix all of ANN coefficients and also a simple procedure to implement our model.

2. The ANN model of the terrestrial bow shock

2.1. The data set

The data set for the development of our ANN consisted of 2944 bow shock crossings from the following spacecraft: IMP1-3-8, EXPLORER-33-34-35, HEOS-1-2, MAGION, GEOTAIL, CLUSTER-1, THEMIS-B and THEMIS-C.

The IMP-1-3, EXPLORER-33-34-35 and HEOS-1-2 crossings came from the original collection which (Formisano, 1979) used to develop the F79 model.

Differently, the IMP-8, GEOTAIL, MAGION and CLUSTER-1 crossings and respective upstream parameters were downloaded from the NSSDCA database http://omniweb.gsfc.nasa.gov/ftpbrowser/bowshock.html.

The list of THEMIS-B and THEMIS-C bow shock crossings was compiled at IAPS-INAF by inspecting the THEMIS/ESA ion spectrograms available at http://themis.ssl.berkeley.edu (an ion spectrogram is a visualization over the time of the energy distribution of the ion count rate measured by the plasma analyzer). Each of the THEMIS crossings was identified in the spectrograms through the spread of the solar wind beam (i.e. the narrow energy band in which the great part of solar wind ion counts are concentrated) to the much more enlarged energy distribution of the counts typically observed downstream in the magnetosheath. Then, each crossing identification was confirmed through the inspection of the jumps in magnetic field magnitude, plasma density, temperature and velocity. The upstream parameters for THEMIS crossings were calculated using plasma and magnetic field data measured by ACE/SWEPAM, ACE/MAG, WIND/3DP and WIND/MFI instruments and available at http://cdaweb.gsfc.nasa.gov.

From the above collection, a training set of 1500 crossings was randomly extracted (Fig.2 shows the angular coverage of the subset). Afterwards, a test set was obtained by selecting, among the remaining 1444 crossings, only the 944 ones not used by (Formisano, 1979) in making his F79 model.

All of the quantitative results reported in the tables and figures of this work can be reproduced on the basis of the algorithms provided in the Appendix and the

test data set available at http://dx.doi.org/10.17632/694773zt2m.2

2.2. The selected network

We choose here to model the bow shock through a simple feedforward network (perceptron) (e.g., Hertz et al., 1991) with four input lines, one hidden layer of five neurons with hyperbolic tangent as activation function and a linear output element (Fig.1). The ANN four inputs are respectively:
the two angular coordinates φ and λ; the radial distance R_{F79} of the bow shock crossing issued by F79 model (for given φ and λ); the upstream solar wind M_a. The ANN output is the predicted radial position R_{ANN} of the bow shock along the same spatial direction (here λ is the latitude in GSE reference frame whereas φ is an azimuthal angle counted counterclockwise from the axis pointing in the opposite direction to X_{GSE}).

The shock radial position R_{F79}, for given solar wind number density N_{obs} and bulk speed V_{obs}, is expressed as:

$$R_{F79} = (\frac{N_0 V_0^2}{N_{obs} V_{obs}^2})^{1/6} R_0 \tag{1}$$

where R_0 is radial distance of the point (with angular coordinates φ and λ) on the Formisano's normalized surface (see Tab.3 of Formisano (1979)). $N_0 = 9.4cm^{-3}$ and $V_0 = 450km/s^{-1}$ are two costants of the F79 model. Therefore, in our model the fundamental dependence of the shock position on the ram pressure of the solar wind P_{ram} is implicitly taken into account via R_{F79} (Eq.1). We consider also the additional input M_a as, among the three Mach numbers, it is the one which seems most clearly to control the shape and asymmetry of the bow shock (Formisano, 1979; Peredo et al., 1995).

The mathematical structure of the ANN is described through the two following formulas. The output of the i-th hidden layer neuron is:

$$x_i = tanh(\sum_{j=1}^{4} w_{ij}^{(1)} u_j), \tag{2}$$

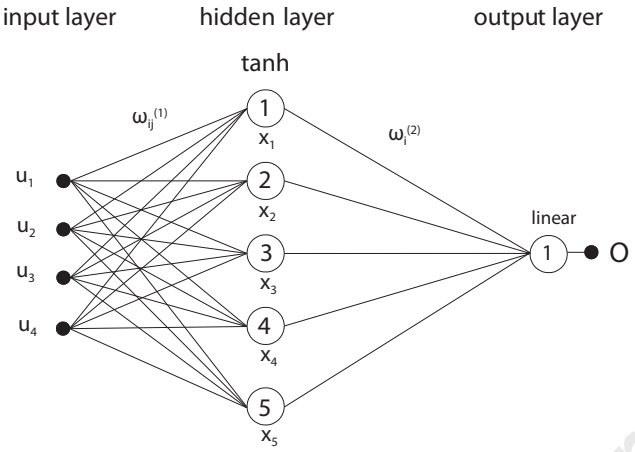

Figure 1: The scheme of the feedforward network used in the present study. The inputs u_1, u_2, u_3 and u_4 are λ, ϕ, R_{F79} and M_a respectively. The hidden neurons have hyperbolic tangent activation functions whereas the output neuron is linear. w's are the network weights.

where the sum is made over the 4 normalized external inputs u_i (see the Appendix for details); $w_{ij}^{(1)}$ are the weights of the connections between the i-th hidden layer neuron and the j-th inputs. Then, the normalized output O is obtained from a linear combination of the 5 hidden layer outputs x_i:

$$O = \sum_{i=1}^{5} w_i^{(2)} x_i, \tag{3}$$

where $w_i^{(2)}$ are the weights of the connections between the output unit and the i-th hidden neuron.

The rationale behind the present work is to illustrate the new ANN approach to the bow shock modeling and its advantages over the traditional surface best-fitting technique. This work aims to provide an effective algorithm as well, not the best although. The choice of F79 model as input to our network is really a suitable one to achieve these goals. As a matter of fact, F79 is a very simple hydrodynamic model depending only on the solar wind ram pressure. Nonetheless, it is a quite satisfactory model (e.g., Merka et al., 2003). Therefore, a successful correction to F79 made through an ANN represents an interesting

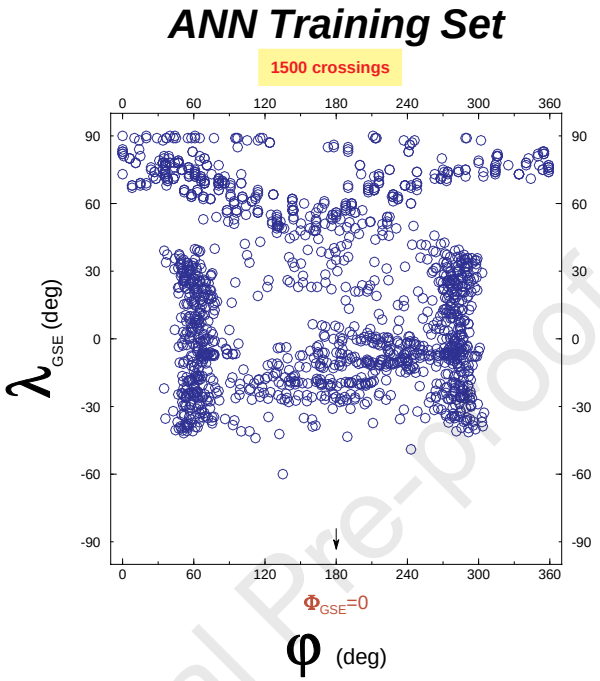

Figure 2: Angular distribution of the bow shock crossings in the training set. λ_{GSE} is the GSE latitude whereas ϕ is an azimuthal angle counted counterclockwise from the opposite axis to X_{GSE}. The crossings come from the observations of the following spacecraft: IMP1-3-8, EXPLORER33-34-35, HEOS1-2, MAGION, GEOTAIL, CLUSTER1, THEMIS-B and THEMIS-C.Notice the absence of crossings in southern hemisphere with latitudes $\lambda_{GSE} < -50°$.

achievement per se, which allows us, moreover, to exemplify how easy is the addition of a new physical parameter (in this case M_a) to an existing model. Also, as shown in section 2.4, the choice of F79 as input to the ANN model permits us to give robust and direct evidence that M_a really plays a role in determining the shock position.

2.3. The training

The ANN weights $w_{ij}^{(1)}$ and $w_i^{(2)}$ were determined by minimizing the cost function:

$$E(w) = 1/2 \sum_{i=1}^{N_{tr}} (T^{(i)} - O^{(i)})^2, \quad (4)$$

where N_{tr} is the number of data points in the training set, $T^{(i)}$ is the radial distance of the i-th observed crossing (i.e. the "right answer" in such supervised learning), and $O^{(i)}$ the corresponding network output. A hybrid scheme in two steps was used to minimize $E(w)$ (Pallocchia et al., 2006). Firstly, the standard algorithm of the error backpropagation (Rumelhart et al., 1986) was applied for a prefixed number of iterations. The weights thus obtained, then, were further modified through a sort of Monte Carlo method in order to prevent the minimization procedure to be stuck in local minima of the hyper-surface $E(w)$ in the space of network weights (see Pallocchia et al. (2006) for further details). The resulting matrices $w_{ij}^{(1)}$ and $w_i^{(2)}$ are reported in Appendix together with the simple procedure to implement the ANN.

2.4. The testing and the comparison with F79

We comparatively tested the performances of the ANN and F79 models over a data set consisting of 944 crossings collected by several spacecraft.

The ratio of the predicted R_{pred} to observed R_{obs} radial distance $r = R_{pred}/R_{obs}$ is the parameter that we chose to evaluate the model performances (Merka et al., 2003). In case of an ideal model $r \equiv 1$. However, r is not constant but varies in case of predictions issued by an algorithm processing real data. Hence, the model accuracy must be evaluated on the basis of the properties of a distribution of values.

The distribution of r is a bell-shaped, approximately Gaussian, when calculated over our collection of crossings (Fig.3). Indeed, very similar distributions of r are found also for several other models (Merka et al., 2003; Jeřáb et al., 2005). This general result indicates that r is a random variable. It follows that, for a given model, any set of observed values of r can be considered as a sample drawn from the statistical population consisting of the whole universe of the r values, viz all the values coming from the predictions of all possible crossings.

In principle, the knowledge of the parameters of such population (i.e. the moments of r probability distribution function: mean, variance, skewness, kurtosis, etc.) would provide us with any information on the model performances. However, those parameters are unknown as we cannot measure the whole (infinite) population. Nonetheless, the statistical inference allows us to draw conclusions about the population parameters through a sample data analysis.

Hence, we assessed the prediction accuracy of both ANN and F79 models and the significance of their differences through the hypothesis testing method of the inferential statistics (terminology, definitions and basic theory concerning the hypothesis tests can be found throughout all elementary statistics textbooks, see, e.g. Hardle et al. (2018)).

By using the Z-statistic with standard normal distribution:

$$Z = \sqrt{N}(\overline{r} - \mu_r)/s_r \tag{5}$$

(where N is the sample size whereas $\mu_r, \overline{r}, s_r$ are the r expected value, sample mean and standard deviation, respectively), we conducted a two-tailed hypothesis test to discover possible biases in both ANN and F79 models, viz a test to infer whether the model predictions were consistent or not with those of a model issuing, on average, the unbiased (i.e. correct) response $\mu_r = 1$. (We deliberately use here the classical term r expected value for μ_r, in place of r population mean, to highlight the inferential character of the test. In fact, the expected value of a random variable is the value that we expect to obtain as result of a sample mean performed over a very large number of experimental values (Law of Great Numbers in statistics).)

Hence, we tested:

$H_0 : \mu_r = 1 \; against \; H_1 : \mu_r \neq 1$.

where H_0 is the null-hypothesis. H_1, complement of H_0, is called alternative hypothesis.

In case of acceptance of H_0 we say the model is unbiased, otherwise it is biased.

In addition, to evalutate the statistical significance of the differences between $\overline{r}_{ANN}$ and $\overline{r}_{F79}$, we tested:

$H_0 : \mu_{r_{ANN}} = \mu_{r_{F79}} \;\; against \;\; H_1 : \mu_{r_{ANN}} \neq \mu_{r_{F79}}$

In this case we used the Z-statistic:

$$Z = \sqrt{N}((\overline{r}_{ANN} - \overline{r}_{F79}) - (\mu_{r_{ANN}} - \mu_{r_{F79}}))/\sqrt{s^2_{rANN} + s^2_{rF79}} \qquad (6)$$

Depending on whether H_0 was accepted or not, we say the models are the same or different.

The chosen significance level for both the above two-sided Z-tests was $\alpha = 0.01$, that is we took a 1% risk to reject a null-hypothesis H_0 when instead it was true (i.e. α is the probability of making a type I error) (e.g. Hardle et al., 2018).

Hence, our decision rule in terms of p-value p_0:

$$if \;\; p_0 \geq \alpha/2 = 0.5\% \;\; then \; H_0 \; accepted \; else \; H_0 \; rejected \qquad (7)$$

In fact, the p-value is the probability of finding the actual, or more extreme, values of the test-statistic under the assumption that the null-hypothesis H_0 is true. These actual values of the test-statistic are dubbed "scores".

The decision rule can be formulated also in terms of confidence interval for the Z-scores Z_0 obtained from equations (5) and (6) as follows:

$$if - Z_{\alpha/2} \leq Z_0 \leq Z_{\alpha/2} \; then \; H_0 \; accepted \; else \; H_0 \; rejected \qquad (8)$$

where $Z_{\alpha/2} = 2.58$ is the score for which the p-value is exactly $p_0 = 0.5\%$.

We complete the description of the Z-tests underlining the probabilistic meaning of the outcome of any hypothesis test. As a matter of fact, we accept the null-hypothesis H_0 if the observed data (in the sample) does not deviate from what would be expected on the basis of chance alone. Thus, we cannot be certain whether H_0 is true or not but we can just decide whether it is likely or not.

Table 1 reports the results of the above statistical analysis performed over the test data set organized in the following way: all crossings; crossings in northern ($Y_{GSE} \geq 0; Z_{GSE} \geq 0$) and southern ($Y_{GSE} \geq 0; Z_{GSE} < 0$) dusk flank, crossings in northern ($Y_{GSE} < 0; Z_{GSE} \geq 0$) and southern ($Y_{GSE} < 0; Z_{GSE} < 0$) dawn flank. The names of these subsets are abbreviated as All, NDuF, SDuF,NDaF and SDaF, respectively.

Looking at the p-values p_0 and Z-scores Z_0 of Table 1 (fifth and sixth column) and remembering the above decision rule (eq.7 or eq.8), we find that the two models differ (i.e. $H_0 : \mu_{r_{ANN}} = \mu_{r_{F79}}$ rejected) and are both biased (i.e. $H_0 : \mu_r = 1$ rejected)) as far as the whole test set All is concerned. However, the ANN predictions are more accurate than those of F79 model as the overestimate of the shock distance is 2.1% in the ANN case whereas it is 5% in F79 case (see the respective $\overline{r}$ in Tab. 1).

The ANN model performs better than F79 also when we evaluate the predictions over the test data grouped by spatial regions. In fact, except for the region NDuF where the hypothesis $H_0 : \mu_{r_{ANN}} = \mu_{r_{F79}}$ is accepted, in the other three regions the differences between the models are significant and the ANN biases (if any) are lower than those of F79 model as $Z_{0_{ANN}} < Z_{0_{F79}}$ (see the respective Z-scores in the fifth column of Tab.1).

The same statistical tests were used also to evalutate the accuracy of both ANN and F79 predictions at varying upstream Alfvénic Mach's number M_a and solar wind ram pressure P_{ram}. The corresponding results are reported in Table 2.

For low $M_a < 5$ and high $M_a \geq 15$ values, the ANN predictions are unbiased (i.e. $H_0 : \mu_{r_{ANN}} = 1$ accepted) (see the respective Z-scores and p-values of the fifth column of Tab. 2) whereas, for $5 \leq M_a < 10$ and $10 \leq M_a < 15$, they are biased by about 2%. Differently, F79 model overestimates or underestimates the shock distances by roughly $6 \div 9\%$ over all considered M_a subsets (see the respective $\overline{r}$ in Tab. 2).

In the case of test data binned by P_{ram}, it is found that for high ($4 \leq P_{ram} < 6\ nPa$) or very high ($P_{ram} \geq 6\ nPa$) values the null-hypothesis $H_0 : \mu_{r_{ANN}} = \mu_{r_{F79}}$ must be accepted. Nonetheless, the ANN predictions are unbiased for $4 \leq P_{ram} < 6\ nPa$ but not for $P_{ram} \geq 6\ nPa$ whereas the F79 ones are unbiased in both subsets (see the respective Z-scores and p-values in Tab.2).

For medium ($2 \leq P_{ram} < 4\ nPa$) ram pressure the ANN and F79 predictions differ (viz $H_0 : \mu_{r_{ANN}} = \mu_{r_{F79}}$ rejected) whereas for lower values ($P_{ram} < 2\ nPa$) no significant difference is found between the model predictions (viz $H_0 : \mu_{r_{ANN}} = \mu_{r_{F79}}$ accepted). Moreover, the ANN predictions are more ac-

curate than F79 ones, albeit both models overestimate the shock position by approximately $2 \div 4\%$ and 6%, respectively (see the respective $\overline{r}$ in Tab. 2).

In addition to the Z-tests conducted to assess the accuracy of the model predictions, we performed a F-test to infer whether the forecast precision of ANN and F79 models was the same or whether the ANN forecast precision was higher than the F79 one. As the population variance σ_r^2 measures the dispersion of r around the mean μ_r (i.e. the mean squared error), we considered $(\sigma_r^2)^{-1}$ as measure of the forecast precision and, therefore, $(s_r^2)^{-1}$ as its best guess calculated from the sample data. Thus, by means of the F-statistic:

$$F = \frac{s^2_{r_{F79}}/\sigma^2_{r_{F79}}}{s^2_{r_{ANN}}/\sigma^2_{r_{ANN}}} \tag{9}$$

we tested the null-hypothesis of equal population variances:

$H_0 : \sigma^2_{r_{ANN}} = \sigma^2_{r_{F79}}$ *against* $H_1 : \sigma^2_{r_{F79}} > \sigma^2_{r_{ANN}}$.

We set the significance level $\alpha = 0.01$ for one-tailed test, so that the decision rule in terms of p-value p_0 was:

$$if\ p_0 \geq 0.1\%\ H_0\ accepted\ else\ H_0\ rejected \tag{10}$$

In case of H_0 acceptance we say that no significant difference in forecast precision is observed. Vice versa, i.e. H_0 rejected in favor of H_1, we say that the ANN model is (likely) more precise than F79 one.

Looking at the p-values p_0 for the F-scores (obtained from eq.9 in the last columns of Table 1 and Table 2) and applying to them the above decision rule (eq.10), we find out that the ANN predictions are effectively more precise than the F79 ones (viz H_0 rejected in favor H_1) for whole set All and for two of four spatial regions indicated in Table 1. This is the case for low and medium ram pressures ($P_{ram} < 4\ nPa$) as well. Differently, for higher pressures ($P_{ram} \geq 4\ nPa$) we find no significant difference (viz H_0 accepted) between the forecast precision of the two models (see Tab.2).

Interestingly enough, we can see that H_0 is always accepted when the F-tests are performed over the test data organized into M_a classes, that is no significant statistical difference is detected between $s^2_{r_{ANN}}$ and $s^2_{r_{F79}}$ (see the corresponding

p-values p_0 in last column of Tab.2). Hence, this result indicates that taking into account M_a in our ANN does not improve the forecast precision in comparison with F79 model (which solely depends on P_{ram}).

The results of the statistical analysis are graphically summarized in Figure 4 where we can notice at a glance that, in most cases, the ANN model performs better than F79 one. For example, looking at the fifth panel of Figure 4, we see that the ANN Z-scores are generally smaller (and several of them are inside the yellow area) that F79 ones and, therefore, that the forecast accuracy of the ANN is higher than forecast accuracy of F79 model.

In order to verify that the upstream Alfvénic Mach's number M_a really does play an important role in forecasting the bow shock position, we built a second network ANN' identical to the initial ANN but without the M_a input line (note ANN' depends only on P_{ram} via F79 input). We trained ANN' over the same data set used for ANN. Moreover, we evaluated the ANN' performances through the same statistical analysis performed for both ANN and F79 models. The results also in this case are summarized in Figure 4.

A direct comparison between ANN' and ANN Z-statistics indicates that the two networks predict the shock distance with the same accuracy (viz $H_0 : \mu_{r_{ANN}} = \mu_{r_{ANN'}}$ accepted) when the test data are grouped by spatial region and P_{ram} or not grouped at all (see bottom panel of Fig.4). On the contrary, we notice that in case of low ($M_a < 5$), high ($10 \leq M_a < 15$) and very high ($M_a \geq 15$) Alfvénic Mach's number, ANN is more accurate than ANN' since the Z-scores $Z_{0_{ANN}}$ are lower than $Z_{0_{ANN'}}$ ones. In addition, two of three $Z_{0_{ANN}}$ are inside the yellow area where the unbiased model hypothesis $H_0 : \mu_{r_{ANN}} = 1$ is accepted (see fifth panel in Fig.4). Only in case of medium M_a values ($5 \leq M_a < 10$) the predictions of the two networks do not significantly differ (see bottom panel of Fig.4).

On the other hand, the F-tests show that the null hypothesis $H_0 : \sigma^2_{r_{ANN'}} = \sigma^2_{r_{ANN}}$ is generally accepted when the test data are arranged into M_a or P_{ram} classes or spatial regions (in fact, except for NDuF region, all of the respective F-scores are inside the yellow area of the fourth panel of Fig.4). For that reason,

we conclude that the width σ_r of r distribution is practically independent from M_a (in this regard we notice, once again, that ANN' depends on $Pram$ but not on M_a).

With regard to ANN' we also point out that its forecasting accuracy is higher than that of F79 model. Indeed, the ANN' scores $Z_{0_{ANN'}}$ have generally smaller values than the corresponding $Z_{0_{F79}}$ (see fifth panel of Fig.4). The variance $\sigma_{r_{ANN'}}$ tends to be smaller than $\sigma_{r_{F79}}$ as well (see F-scores in fourth panel of Fig.4).

Figure 5 shows the intersections of ANN shock surface with the GSE coordinate planes for different M_a and a fixed typical P_{ram}. For purpose of comparison, the corresponding profiles of the F79 model are also reported. We point out that when M_a increases the ANN shock shape becomes more swept-back. This is qualitatively consistent with the progressive reduction of the Alfvénic Mach cone angle $\theta_a = \arcsin(M_a^{-1})$ for faster and faster flows.

It is worth noting that, for a given increment ΔM_a, this reduction of θ_a becomes gradually smaller when M_a increases as $\Delta\theta_a \approx -M_a^{-2}\Delta M_a$ is a decreasing function of M_a. Such simple result could explain the reason why, in Figure 5 we hardly see any difference in shock position between $M_a = 10$ and $M_a = 15$, while a significant difference is found between $M_a = 5$ and $M_a = 10$ although $\Delta M_a = 5$ is the same in both cases.

Variations in M_a affect also the standoff distance of the ANN bow shock. In fact, for medium and high M_a the model shock is closer to the Earth whereas for low M_a it is found further sunward. From a physical point of view such prediction is reasonable. As a matter of fact, a wave, generated by the solar wind hitting the magnetosphere obstacle, will travel in a given steepening time (i.e. the characteristic time for shock formation) an outward distance proportional to its speed relative to the inward solar wind flow. It follows that the higher the solar wind Mach number is, the closer to Earth the shock is.

Looking at the first two panels of Figure 5, we see, approximately for $X_{GSE} < -15\ R_E$, noticeable differences between the F79 and ANN shock profiles ($M_a = 10, 15$), while the differences are smaller for the $X_{GSE} > -15 R_E$. In this respect,

we recall that Formisano (1979) used for the development of F79 model a data set in which the crossings in the near tail (i.e. the crossings from Explorer33 and Explorer35) were mostly at $X_{GSE} < -20\ R_E$. The ANN training set, instead, contains also a large number of IMP8 crossings observed at $X_{GSE} \simeq -25\ R_E$. Therefore, those significant differences in near tail can be reasonably explained on the basis of an underfitting problem of the F79 model due to the lack of crossings below $X_{GSE} < -20\ R_E$ in Formisano (1979) collection of crossings.

Lastly, we point out that ANN shock shows at very high latitude a discontinuous change in shape. The jump is noticeable especially for low M_a and in the northern part where it can reach some Earth's radii. Interestingly enough, such feature is consistent with a physical picture, suggested by Jelínek et al. (2008), in which the indentation of the magnetopause induces a shock distortion, near the dawn-dusk meridian with width of few Re in Z_{GSM} direction, that moves sunward when the tilt angle increases.

We conclude the section with a note about the limits on validity of the ANN model. As a matter of fact, we trained our ANN over a training set in which there are no crossings with latitude below $\lambda_{GSE} \sim -50°$ (see Fig.2). The same lack of observations in southern hemisphere characterizes also the data set on which Formisano (1979) developed the F79 model which feeds our ANN (see Tab.2 of Formisano (1979)). Hence, although the artificial neural networks have generalization capability (i.e. the ability to handle unseen data), we believe that ANN predictions in the southern hemisphere, at higher latitudes far below $\lambda_{GSE} \sim -50°$ threshold, could be less reliable. Moreover, we cannot trust the ANN predictions for tail regions far beyond $X_{GSE} \simeq -25$ (R_E) where the validity of F79 input could be questionable (Formisano, 1979).

3. Discussion

For a given direction, the present ANN computes the radial distance of the bow shock using R_{F79} and the upstream Alfvénic Mach's number M_a as inputs. As R_{F79} is one of the network inputs, our model can be regarded as a correction

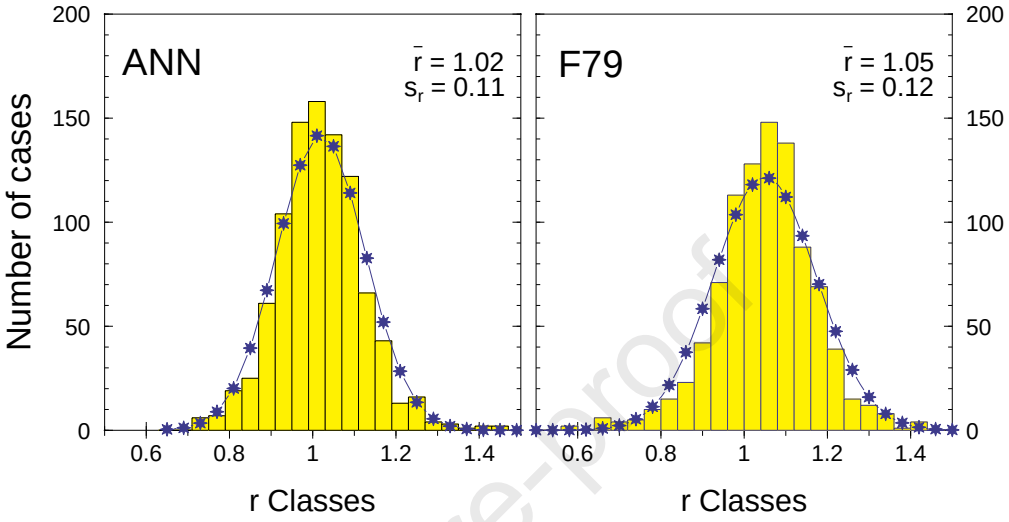

Figure 3: Histograms representing the frequency distributions over the test set of the ratio of the predicted R_{pred} to observed R_{obs} shock radial distance $r = R_{pred}/R_{obs}$ for the ANN (left panel) and F79 (right panel) models. In each of two panels, blue markers are the expected frequencies from a Gaussian distribution having as parameters the sample mean $\overline{r}$ and the standard deviation s_r. The test set consists of $N = 944$ bow shock crossings.

to F79 model. We point out that such correction does not rely on any a priori assumption about the shock shape and its mathematical dependence upon the upstream parameters P_{ram} and M_a. The present study aims to highlight the appealing flexibility of the artificial neural network approach to the empirical modelling of the bow shock surface. We believe that ANN tools might be fruitfully exploited to refine even other bow shock or magnetopause models reported in the literature. However, as we discuss below, the observations raise doubts on the possibility of making advances in practical bow shock modelling beyond a certain threshold.

The sample standard deviation of the random variable r_{ANN} is typically $s_{r_{ANN}} \simeq 0.1$ (Tab.1 and Fig.4). In addition, as shown in previous section, $s_{r_{ANN}}$ can be generally considered equal or very close to the standard deviation $s_{r_{ANN'}}$ re-

lated to the predictions issued by the network ANN' (identical to ANN but without the M_a input line) on the basis only of the solar wind ram pressure P_{ram}. Interestingly enough, values very similar to $s_{r_{ANN}}$ characterize other bow shock models which take into account not only P_{ram} and M_a but also different upstream parameters or the magnitude and direction of the interplanetary magnetic field (see Tab.1 and Tab.2 of Merka et al. (2003) and Fig.9 and Fig.10 of Merka et al. (2005)). Apparently, therefore, a more accurate physical description of the external conditions does not permit the shock models to substantially reduce the statistical dispersion of the variable r around its mean value. A possible explanation might be that the bow shock position is partly unpredictable on the basis of the upstream solar wind parameters only. In this regard, we point out that the bow shock is far from being stationary with respect to the Earth. In fact, shock motions, with speeds ranging from several tens to few hundreds of kilometers per second, are frequently observed (Guha et al., 1972; Formisano et al., 1973; Lepidi et al., 1996; Horbury et al., 2002; Šafránková et al., 2003). The present ANN and all of the aformentioned empirical models, instead, rely tacitly on the assumption that the bow shock is always at rest in its equilibrium state, and, therefore, the shock position can be uniquely derived from the knowledge of the external solar wind conditions. It follows that, in many cases, the predicted bow shock locations may markedly differ from the observed ones as result of the displacements of the shock surface induced by the above motions. Formisano and Mastrantonio (1975) found, according to a Völk and Auer (1974) theoretical result, observational indications that the impact of tangential discontinuities (TD) on the bow shock is probably the main cause of the shock motions. Those authors also found that there is a sufficient number of large TD in the solar wind (an average occurence rate of around 0.5 per hour) to account for the observed speeds of the bow shock greater than 50 km/s. Most recent and direct observations, and MHD simulations clearly showed that the impacts of interplanetary discontinuities and shocks on the magnetosphere cause transient bow shock motions with speed up to several tens of kilometers per second and lasting several minutes (e.g.,

Maynard et al., 2007; Šafránková et al., 2007; Přech et al., 2008; Keika et al., 2009; Pallocchia et al., 2010; Meziane et al., 2014). It follows that the bow shock displacements from the equilibrium position may even reach values of some R_E, viz values comparable to the standard deviation of the predicted bow shock distance R_{pred}. In such interpretive scheme, therefore, the transient bow shock motions act like a noise background which strongly limits the prediction capability of any model. We believe that future advances in bow shock modelling will necessarily depend on the use of carefully selected data sets not containing, as possible, crossings observed shortly afterwards the arrival of interplanetary discontinuities.

4. Summary and conclusions

In this paper we present an empirical bow shock model based on an artificial neural network (ANN) consisting of a perceptron with four input lines, one hidden layer of five neurons and an output of one linear unit. Such ANN computes the radial distance of the bow shock along a given spatial direction, using as input parameters the two angular coordinates of this direction, the corresponding radial bow shock distance R_{F79} issued by Formisano's F79 model and the upstream Alfvénic Mach's number M_a. The fact that R_{F79} is one of the network inputs permits to consider the present ANN as a correction to F79 model.

The accuracy of both ANN and F79 models was evaluated by means of the ratio of predicted to observed radial distance of the bow shock $r = R_{pred}/R_{obs}$. Hypothesis tests were performed at a significance level of 0.01 (i.e. 1% or less chance) to discover possible biases of the model output and also to evaluate the statistical significance of the differences between the ANN and F79 predictions. A second artificial network without the M_a input was trained and tested for purpose of comparison as well.

The results of the analysis can be summarized as follows:

1) The ANN predictions are more accurate and unbiased than F79 ones as

demonstrated through the Z-tests and F-test performed over a large test data set (944 crossings from several spacecraft) grouped by spatial region, upstream Alfvénic Mach's number M_a and solar wind ram pressure P_{ram} classes.

2) M_a is really a relevant parameter to bow shock modelling. Indeed, the ANN performs better than a second network identical to the model in all respects except for the absence of M_a input line.

3) For low M_a, the model bow shock shape is distorted at very high latitudes near the dawn-dusk meridian. Such feature is consistent with a possible tilt-angle effect on the shock geometry as suggested by some past observations.

4) The sample standard deviation of $r = R_{pred}/R_{obs}$ is typically $s_{r_{ANN}} \simeq 0.1$, a value quite close to those found for F79 and some other models based on different set of upstream parameters. By virtue of this similarity, we speculate that an irreducible uncertainty in shock position forecasting originates from the bow shock motions rather than from physical limitations of the models. Using a simple argument we suggest that the impacts of interplanetary discontinuities on the bow shock might account for such common dispersion around the average $\overline{r}$.

5. Acknowledgments

The authors would like to thank J.A. Slavin for making available to them the bow shock crossings from IMP1-3, EXPLORER33-34-35 and HEOS1-2 and the NSSDC teams for providing online public access to their database of crossings (http://omniweb.gsfc.nasa.gov/ftpbrowser/bowshock.html).

The authors would like to thank also ACE/SWEPAM, ACE/MAG, WIND/3DP, WIND/MFI and THEMIS/ESA teams for making their data available and CDAWEB team for providing online public access to ACE and WIND data (http://cdaweb.gsfc.nasa.gov).

Authors special thanks go to D.Ambrosino.

This work has been partially supported by Agenzia Spaziale Italiana (ASI) under contract ASI-INAF I/023/09/0.

Appendix A. The ANN algorithm

The present ANN algorithm is implemented through the following steps:

1) get four input data: φ, λ, R_{F79}, M_a

2) compute $\mathbf{u} = (u_1, u_2, u_3, u_4)^T = (\tilde{\varphi}, \tilde{\lambda}, \tilde{R}_{F79}, \tilde{M}_a)^T$

3) compute $\mathbf{x} = tanh(\omega^{(1)}\mathbf{u})$

4) compute $R = N_R\omega^{(2)}\mathbf{x}$

5) goto 1

The inputs $\tilde{\varphi}$, $\tilde{\lambda}$, $\tilde{R}_{F79}$, $\tilde{M}_a$ are the normalized quantities:

$\tilde{\varphi} = (\varphi - \pi)/N_\varphi$

$\tilde{\lambda} = \lambda/N_\lambda$

$\tilde{R}_{F79} = R_{F79}/N_{R_{F79}}$

$\tilde{M}_a = M_a/N_{M_a}$

(see Section 2.2 for the definitions of φ, λ and R_{F79}).

Both φ and λ must be expressed in radians whereas R_{F79} in Earth's radii R_E ($1R_E = 6378\ km$).

The normalization factors are:

$N_\varphi = \pi/2$

$N_\lambda = \pi/2$

$N_{R_{F79}} = 25.0$

$N_{M_a} = 10.0$

$N_R = 25.0$

whereas the weights of ANN connections are:

$$\omega^{(1)} = \begin{pmatrix} 0.008344 & 0.004120 & 1.033031 & 0.036481 \\ -0.014264 & 0.006845 & 0.157504 & -0.091376 \\ 0.006663 & 0.003041 & 0.150952 & 0.053570 \\ 0.014344 & -0.420579 & 1.282251 & 1.543072 \\ 0.065933 & 0.220703 & -0.600629 & -2.114158 \end{pmatrix}$$

$$\omega^{(2)} = \begin{pmatrix} 0.445582 & 1.831838 & 2.941409 & 2.168403 & 2.255122 \end{pmatrix}$$

For the sake of completeness, we also provide the connection weights of the network ANN′ built to calculate the bow shock position using φ, λ and R_{F79} only. The procedure for obtaining the ANN′ output is the same as that described above.

$$\omega'^{(1)} = \begin{pmatrix} 0.000850 & 0.013762 & 0.023227 \\ -0.007476 & -0.086636 & 0.613271 \\ 0.000762 & 0.014249 & 0.021548 \\ -0.007975 & -0.087253 & 0.614663 \\ 0.000130 & 0.001627 & 0.014889 \end{pmatrix}$$

$$\omega'^{(2)} = \begin{pmatrix} 0.803606 & 0.428658 & 0.763494 & 0.504943 & 30.771233 \end{pmatrix}$$

Binsack, J.H., Vasyliunas, V.M., 1968. Simultaneous IMP 2 and OGO 1 observations of bow shock compression. J. Geophys. Res. 73, 429. doi:10.1029/JA073i001p00429.

Cairns, I.H., Grabbe, C.L., 1994. Towards an MHD theory for the standoff distance of Earth's bow shock. Geophys. Res. Lett. 21, 2781–2784. doi:10.1029/94GL02551.

Cairns, I.H., Lyon, J.G., 1995. MHD simulations of Earth's bow shock at low Mach numbers: Standoff distances. J. Geophys. Res. 100, 17173–17180. doi:10.1029/95JA00993.

Caudill, M., 1989. Neural Network Primer: Part I. AI Expert.

Cybenko, G., 1989. Approximation by superpositions of a sigmoidal function. Mathematics of Control, Signals, and Systems 2, 303–314. URL: www.scopus.com. cited By :6110.

Fairfield, D.H., 1971. Average and unusual locations of the Earth's magnetopause and bow shock. J. Geophys. Res. 76, 6700. doi:10.1029/JA076i028p06700.

Farris, M.H., Russell, C.T., 1994. Determining the standoff distance of the bow shock: Mach number dependence and use of models. J. Geophys. Res. 99, 17681. doi:10.1029/94JA01020.

Formisano, V., 1979. Orientation and shape of the earth's bow shock in three dimensions. Planet. Space Sci. 27, 1151–1161. doi:10.1016/0032-0633(79)90135-1.

Formisano, V., Hedgecock, P.C., Moreno, G., Palmiotto, F., Chao, J.K., 1973. Solar wind interaction with the Earth's magnetic field: 2. Magnetohydrodynamic bow shock. J. Geophys. Res. 78, 3731. doi:10.1029/JA078i019p03731.

Formisano, V., Mastrantonio, G., 1975. On the earth's bow shock motion and speed. Space Sci. Rev. 17, 781–786. doi:10.1007/BF00777255.

Guha, J.K., Judge, D.L., Marburger, J.H., 1972. Ogo 5 magnetic-field data near the Earth's bow shock: A correlation with theory. J. Geophys. Res. 77, 604. doi:10.1029/JA077i004p00604.

Hardle, W.K., Klinke, S., Ronz, B., 2018. Introduction to Statistics: Using Interactive Mm*stat Elements. Springer Publishing Company, Incorporated.

Hertz, J., Krogh, A., Palmer, R.G., 1991. Introduction to the theory of neural computation. Santa Fe Institute Studies in the Sciences of Complexity; Lecture Notes: Addison-Wesley, Redwood City, USA.

Horbury, T.S., Cargill, P.J., Lucek, E.A., Eastwood, J., Balogh, A., Dunlop, M.W., Fornacon, K.H., Georgescu, E., 2002. Four spacecraft measurements of the quasiperpendicular terrestrial bow shock: Orientation and motion. J. Geophys. Res. 107, 1208. doi:10.1029/2001JA000273.

Hornik, K., Stinchcombe, M., White, H., 1989. Multilayer feedforward networks are universal approximators. Neural Networks 2, 359–366. URL: www.scopus.com. cited By :9756.

Jelínek, K., němeček, Z., Šafránková, J., Merka, J., 2008. Influence of the tilt angle on the bow shock shape and location. J. Geophys. Res. (Space Physics) 113, A05220. doi:10.1029/2007JA012813.

Jeřáb, M., Němeček, Z., Šafránková, J., Jelínek, K., Měrka, J., 2005. Improved bow shock model with dependence on the IMF strength. Planet. Space Sci. 53, 85–93. doi:10.1016/j.pss.2004.09.032.

Keika, K., Nakamura, R., Baumjohann, W., Angelopoulos, V., Kabin, K., Glassmeier, K.H., Sibeck, D.G., Magnes, W., Auster, H.U., Fornaçon, K.H., McFadden, J.P., Carlson, C.W., Lucek, E.A., Carr, C.M., Dandouras, I., Rankin, R., 2009. Deformation and evolution of solar wind discontinuities through their interactions with the Earth's bow shock. J. Geophys. Res. (Space Physics) 114, A00C26. doi:10.1029/2008JA013481.

Lepidi, S., Villante, U., Lazarus, A.J., Szabo, A., Paularena, K., 1996. Observations of bow shock motion during times of variable solar wind conditions. J. Geophys. Res. 101, 11107–11124. doi:10.1029/96JA00478.

Maynard, N.C., Burke, W.J., Ober, D.M., Farrugia, C.J., Kucharek, H., Lester, M., Mozer, F.S., Russell, C.T., Siebert, K.D., 2007. Interaction of the bow shock with a tangential discontinuity and solar wind density decrease: Observations of predicted fast mode waves and magnetosheath merging. J. Geophys. Res. (Space Physics) 112, A12219. doi:10.1029/2007JA012293.

Merka, J., Szabo, A., Narock, T.W., King, J.H., Paularena, K.I., Richardson, J.D., 2003. A comparison of IMP 8 observed bow shock positions with model predictions. J. Geophys. Res. 108, 1077. doi:10.1029/2002JA009384.

Merka, J., Szabo, A., Slavin, J.A., Peredo, M., 2005. Three-dimensional position and shape of the bow shock and their variation with upstream Mach numbers

and interplanetary magnetic field orientation. J. Geophys. Res. 110, 4202. doi:10.1029/2004JA010944.

Meziane, K., Alrefay, T.Y., Hamza, A.M., 2014. On the shape and motion of the Earth's bow shock. Planet. Space Sci. 93, 1–9. doi:10.1016/j.pss.2014.01.006.

Nemecek, Z., Safrankova, J., 1991. The earth's bow shock and magnetopause position as a result of the solar wind-magnetosphere interaction. J. Atmos. Terr. Phys. 53, 1049–1054.

Pallocchia, G., Amata, E., Consolini, G., Marcucci, M.F., Bertello, I., 2006. Geomagnetic D_{st} index forecast based on IMF data only. Ann. Geophys. 24, 989–999. doi:10.5194/angeo-24-989-2006.

Pallocchia, G., Samsonov, A.A., Bavassano Cattaneo, M.B., Marcucci, M.F., Rème, H., Carr, C.M., Cao, J.B., 2010. Interplanetary shock transmitted into the Earth's magnetosheath: Cluster and Double Star observations. Ann. Geophys. 28, 1141–1156. doi:10.5194/angeo-28-1141-2010.

Peredo, M., Slavin, J.A., Mazur, E., Curtis, S.A., 1995. Three-dimensional position and shape of the bow shock and their variation with Alfvenic, sonic and magnetosonic Mach numbers and interplanetary magnetic field orientation. J. Geophys. Res. 100, 7907–7916. doi:10.1029/94JA02545.

Přech, L., Němeček, Z., Šafránková, J., 2008. Response of magnetospheric boundaries to the interplanetary shock: Themis contribution. Geophys. Res. Lett. 35, 17. doi:10.1029/2008GL033593.

Rumelhart, D.E., Hinton, G.E., Williams, R.J., 1986. Learning representations by back-propagating errors. Nature 323, 533–536. doi:10.1038/323533a0.

Seiff, A., 1962. Recent Information on Hypersonic Flow Fields. NASA Special Publication 24, 19.

Spreiter, J.R., Summers, A.L., Alksne, A.Y., 1966. Hydromagnetic flow around the magnetosphere. Planet. Space Sci. 14, 223. doi:10.1016/0032-0633(66)90124-3.

Šafránková, J., Jelínek, K., Němeček, Z., 2003. The bow shock velocity from two-point measurements in frame of the interball project. Adv. Space Res. 31, 1377–1382.

Šafránková, J., Němeček, Z., Přech, L., Samsonov, A.A., Koval, A., Andréeová, K., 2007. Modification of interplanetary shocks near the bow shock and through the magnetosheath. J. Geophys. Res. 112, 8212. doi:10.1029/2007JA012503.

Verigin, M., Kotova, G., Szabo, A., Slavin, J., Gombosi, T., Kabin, K., Shugaev, F., Kalinchenko, A., 2001. Wind observations of the terrestrial bow shock: 3-D shape and motion. Earth, Planets, and Space 53, 1001–1009.

Völk, H.J., Auer, R.D., 1974. Motions of the bow shock induced by interplanetary disturbances. J. Geophys. Res. 79, 40. doi:10.1029/JA079i001p00040.

Model	Class (# pts)	$\overline{r}$	s_r	$Z_0 = \frac{\sqrt{N}(\overline{r}-1)}{s_r}$ (p_0)	$Z_0 = \frac{\sqrt{N}(\overline{r}_{ANN}-\overline{r}_{F79})}{\sqrt{s^2_{r_{ANN}}+s^2_{r_{F79}}}}$ (p_0)	$F_0 = \frac{s^2{}_{r_{F79}}}{s^2{}_{r_{ANN}}}$ (p_0)
ANN	All (944)	1.021	0.105	6.14 (0.00%)	−5.51 (0.00%)	1.37 (0.00%)
F79		1.050	0.123	12.49 (0.00%)		
ANN	NDuF (203)	1.035	0.109	4.57 (0.00%)	−1.81 (3.51%)	1.51 (0.18%)
F79		1.057	0.134	6.06 (0.00%)		
ANN	SDuF (320)	1.017	0.098	3.10 (0.01%)	−3.14 (0.08%)	1.28 (1.39%)
F79		1.043	0.111	6.93 (0.00%)		
ANN	NDaF (188)	1.026	0.114	3.13 (0.09%)	−3.13 (0.09%)	1.24 (7.11%)
F79		1.065	0.127	7.02 (0.00%)		
ANN	SDaF (233)	1.012	0.104	1.76 (3.92%)	−2.94 (0.16%)	1.40 (0.53%)
F79		1.043	0.123	5.34 (0.00%)		

Table 1: The sample mean $\overline{r}$ and standard deviation s_r of the prediction variable $r = R_{pred}/R_{obs}$ calculated over all the bow shock crossings of the test set (All) and over four subsets corresponding to crossings observed in the spatial regions: (NDuF) northern ($Y_{GSE} \geq 0; Z_{GSE} \geq 0$) and (SDuF) southern ($Y_{GSE} \geq 0; Z_{GSE} < 0$) dusk flank, (NDaF) northern ($Y_{GSE} < 0; Z_{GSE} \geq 0$) and (SDaF) southern ($Y_{GSE} < 0; Z_{GSE} < 0$) dawn flank. In the last three columns are reported the Z-scores and F-scores used to test the null hypotheses $H_0 : \mu_r = 1$, $H_0 : \mu_{r_{ANN}} = \mu_{r_{F79}}$ and $H_0 : \sigma^2_{r_{ANN}} = \sigma^2_{r_{F79}}$ (μ_r and σ^2_r are the expected value and the variance of the random variable r). The p-values p_0 are calculated from the standard normal and F distributions. The chosen significance level is $\alpha = 0.01$, so that the null hypotheses are accepted if $p_0 \geq 0.5\%$ in the two-tailed Z-tests or $p_0 \geq 1.0\%$ in the one-tailed F-test, otherwise they are rejected in favor of the alternative ones: $H_1 : \mu_r \neq 1$; $H_1 : \mu_{r_{ANN}} \neq \mu_{r_{F79}}$ and $H_1 : \sigma^2_{r_{F79}} > \sigma^2_{r_{ANN}}$.

Model	Class (# pts)	$\overline{r}$	s_r	$Z_0 = \frac{\sqrt{N}(\overline{r}-1)}{s_r}$ (p_0)	$Z_0 = \frac{\sqrt{N}(\overline{r}_{ANN}-\overline{r}_{F79})}{\sqrt{s^2{}_{r_{ANN}}+s^2{}_{r_{F79}}}}$ (p_0)	$F_0 = \frac{s^2_{r_{F79}}}{s^2_{r_{ANN}}}$ (p_0)
ANN	$M_a < 5$ (93)	1.030	0.161	1.80 (3.59%)	3.59 (0.02%)	1.41 (5.06%)
F79		0.937	0.191	−3.18 (0.07%)		
ANN	$5 \leq M_a < 10$ (473)	1.021	0.099	4.61 (0.00%)	−4.58 (0.00%)	1.21 (1.93%)
F79		1.052	0.109	10.38 (0.00%)		
ANN	$10 \leq M_a < 15$ (279)	1.021	0.093	3.77 (0.00%)	−6.37 (0.00%)	1.07 (28.66%)
F79		1.072	0.096	12.53 (0.00%)		
ANN	$M_a \geq 15$ (99)	1.019	0.105	1.80 (3.59%)	−4.34 (0.00%)	1.14 (25.89%)
F79		1.086	0.112	7.64 (0.00%)		
ANN	$P_{ram} < 2$ (505)	1.04	0.097	9.27 (0.00%)	−2.51 (0.6%)	1.45 (0.00%)
F79		1.057	0.117	10.95 (0.00%)		
ANN	$2 \leq P_{ram} < 4$ (319)	1.018	0.103	3.12 (0.09%)	−4.77 (0.00%)	1.33 (0.56%)
F79		1.060	0.119	9.01 (0.00%)		
ANN	$4 \leq P_{ram} < 6$ (71)	0.982	0.110	−1.38 (8.38%)	−2.37 (0.87%)	1.40 (8.09%)
F79		1.030	0.130	1.94 (2.62%)		
ANN	$P_{ram} \geq 6$ (49)	0.911	0.111	−5.61 (0.00%)	−1.43 (7.64%)	1.80 (2.21%)
F79		0.949	0.149	−2.40 (0.82%)		

Table 2: Same format as Table 1 but for test crossings grouped into upstream Alfvénic Mach's number M_a and ram pressure P_{ram} classes .

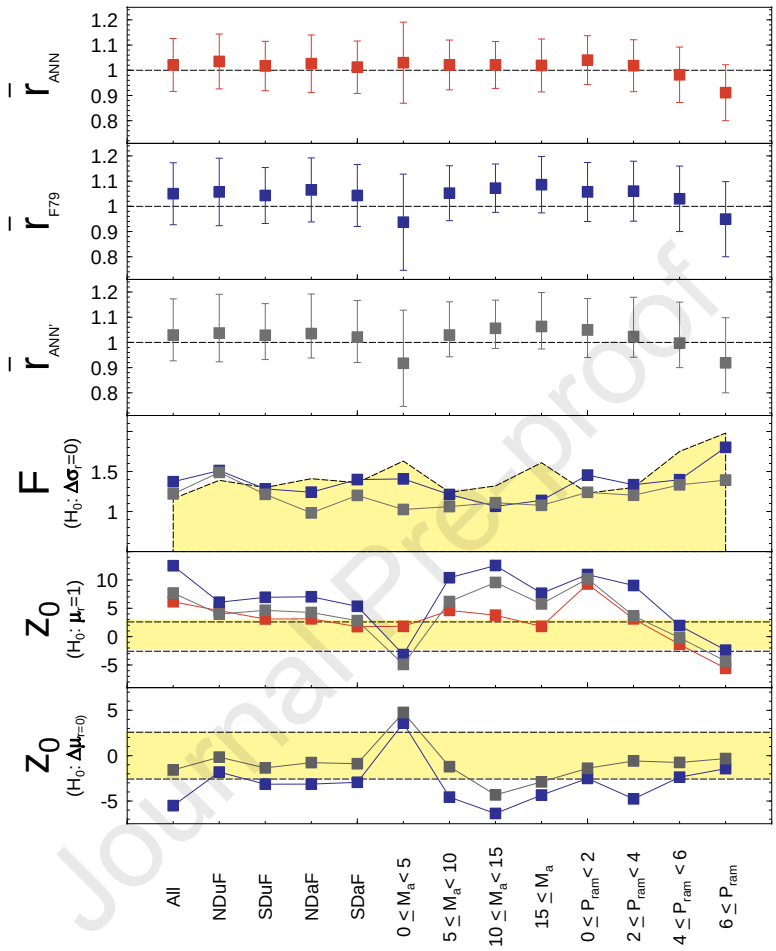

Figure 4: Graphical summary of the statistical results of Tab.1 and Tab.2 concerning the ANN and F79 models. The results pertaining to the ANN' network are reported as well. In the three upper panels the sample means calculated over the indicated subsets. The horizontal dashed lines correspond $\mu_r = 1$, i.e. the expected value for an unbiased model. The error bars are given by the sample standard deviations s_r. In the fourth panel the F-statistic values (F-scores) calculated to test the null hypotheses $H_0 : \sigma^2_{r_{ANN}} = \sigma^2_{r_{F79}}$ (blue) and $H_0 : \sigma^2_{r_{ANN}} = \sigma^2_{r_{ANN'}}$ (grey). In the lower two panels the Z-statistic values (Z-scores) to test the null hypotheses $H_0 : \mu_r = 1$ (same colors as the three upper panels), $H_0 : \mu_{r_{ANN}} = \mu_{r_{F79}}$ (blue) and $H_0 : \mu_{r_{ANN}} = \mu_{r_{ANN'}}$ (grey). A test-score inside a yellow area means that the respective H_0 is accepted at 1% significance level.

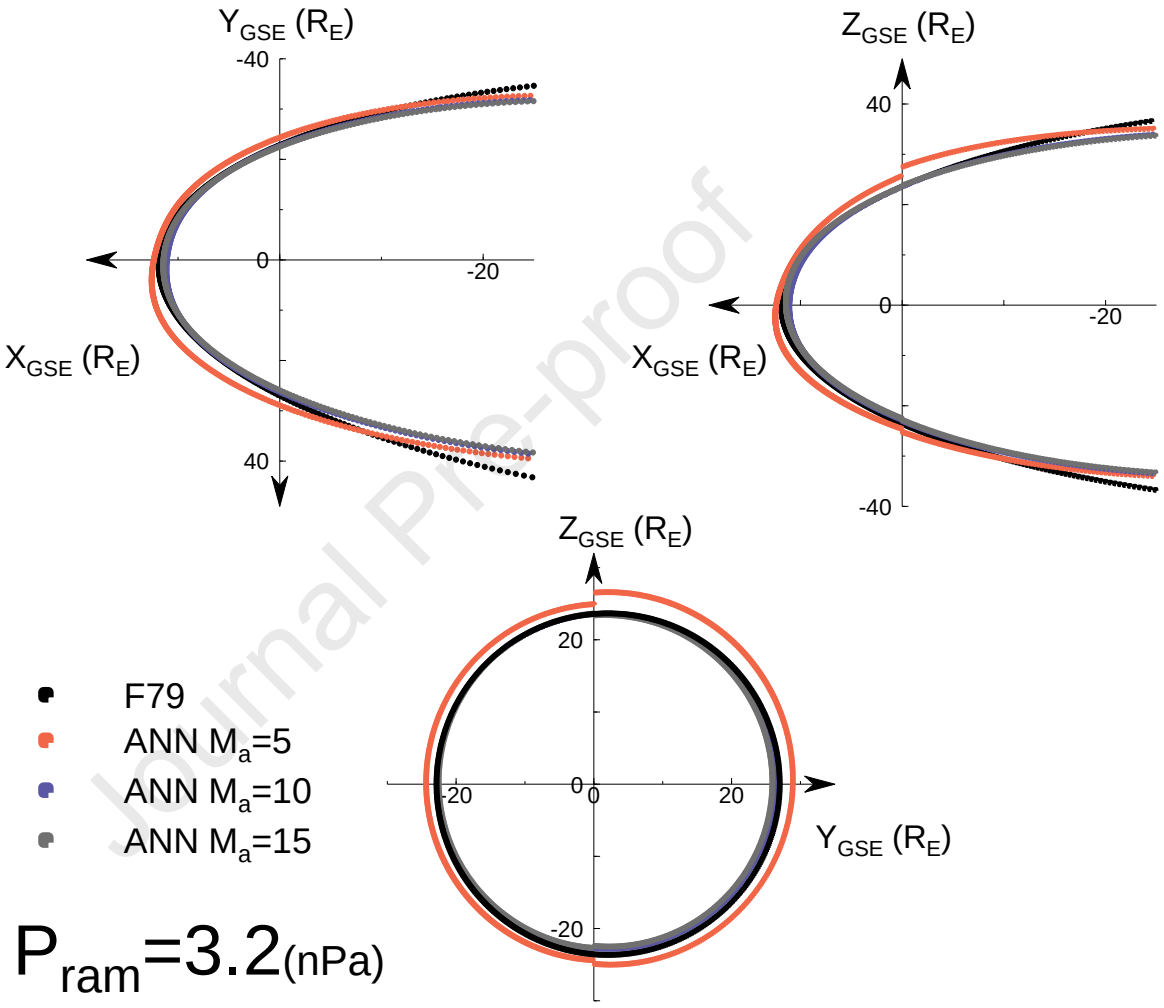

Figure 5: The intersections of the ANN bow shock with the GSE coordinate planes for three different values of Alfvénic Mach's number M_a and for a typical value of the solar wind ram pressure P_{ram}. For purpose of comparison, the curves corresponding to the F79 model are plotted as well.

- Artificial neural network: a novel and powerful approach to the bow shock modelling
- An effective correction to the Formisano's bow shock model
- Clear evidence that alfvénic Mach number is relevant to the bow shock modelling

Declaration of interests

The authors declare that they have no known competing financial interests or personal relationships that could have appeared to influence the work reported in this paper.